

# Natural Gauge Fields in Propagating Polariton Superfluids

H. Terças,<sup>1</sup> H. Flayac,<sup>1,2</sup> D. D. Solnyshkov,<sup>1</sup> and G. Malpuech<sup>1</sup>

<sup>1</sup>*Institut Pascal, PHOTON-N2, Clermont Université, Blaise Pascal University, CNRS, 24 Avenue des Landais, 63177 Aubière Cedex, France*

<sup>2</sup>*Institute of Theoretical Physics, École Polytechnique Fédérale de Lausanne EPFL, CH-1015 Lausanne, Switzerland*

We show that the interplay between the structure anisotropy and the energy splitting between the TE and TM modes of a microcavity leads to the appearance of a gauge field for a propagating polariton condensate. The field texture can be tuned by rotating the sample and ranges continuously from a Rashba to a monopolar field. In the linear regime, the monopolar field leads to a remarkable focusing effect. In the interacting regime, the spin-orbit coupling induces a breakdown of superfluidity. The spatially homogeneous flows become unstable and dynamically evolve into textured ground states such as stripes and domain walls.

The creation of synthetic gauge fields has been seriously addressed in the last years [1–4]. In condensed matter systems, spin-orbit coupling (SOC) plays a central role in the spin-Hall effect [5, 6], topological insulators [7, 8] and semiconductor-based spintronics [9]. The creation of synthetic magnetic fields in atomic Bose-Einstein condensates (BECs) has allowed the formation of vortices without stirring [1], while the fabrication of a synthetic gauge field of the Rashba type leads to the formation of spin domains [2]. In semiconductor microcavities, both photons and strongly coupled exciton-polaritons experience a spin-orbit coupling. It originates from the splitting between TE and TM modes corresponding to an effective magnetic field [10, 11] with a quadratic dependence over  $k$  and a  $2\theta$  azimuthal dependence. An additional splitting between linear polarizations at  $k = 0$  corresponds to a constant magnetic field associated with the crystallographic axes [12]. While the TE-TM field leads to several fascinating effects, such as the optical spin-Hall effect [13–15] or the acceleration of magnetic monopole analogs [16, 17], it cannot be integrated in the Hamiltonian as a minimal coupling. In other words, alone, it does not exhibit the properties of a true gauge field satisfying gauge transformations. The dispersion of the elementary excitations of a polariton BEC in the presence of the TE-TM splitting is anisotropic [18], but the dynamics of the condensate is completely stable. The physical reason is that the TE-TM field does not break the time-reversal symmetry [19], contrary to what happens in the Rashba/Dresselhaus field [20, 21]. The effect of trapping has also been discussed in the context of SOC atomic BECs: As a result of the parametric instability occurring at  $k = 0$ , the ground state of the system is found to demonstrate either stripes or vortices, rather than the Thomas-Fermi profile [22]. In contrast, the TE-TM field in polariton BECs allow for a homogeneous (phase mixed) ground state.

In this Letter, we show that the situation can be dramatically changed when the polariton condensate is put in motion. Under typical experimental situations, the condensate can be loaded at a controlled wavevector  $\mathbf{k}_0$  by simply adjusting the angles between the laser beam

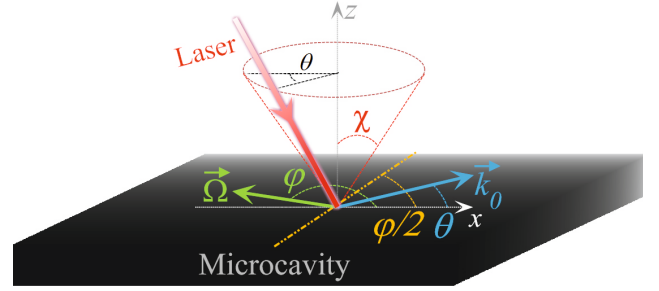


FIG. 1: (color online). Schematics of the experimental configuration necessary to produce a controllable polaritonic gauge field in a microcavity. The angle between the crystallographic axis (the effective magnetic field  $\Omega$ ) and the horizontal is  $\varphi/2$  ( $\varphi$ ). A laser with a vertical inclination  $\chi$  and making an angle of  $\theta$  with the horizontal produces a propagating polariton beam with wave-vector  $\mathbf{k}_0 = (\omega_0/c) \sin \chi (\cos \theta, \sin \theta)$ , where  $\omega_0$  is the laser frequency and  $c$  is the light speed.

and the normal and horizontal axes of the cavity (see Fig. 1). At a critical velocity  $\mathbf{v}_* = \hbar \mathbf{k}_*/m$ , for which the static  $\Omega$  and TE-TM fields exactly compensate, the dynamics of the low-wavevector excitations is governed by a natural gauge field of the Rashba kind. In the present discussion,  $\Omega = \Omega(\cos \varphi, \sin \varphi)$  describes an effective in-plane magnetic field associated with the crystallographic axis [10], as illustrated in Fig. 1. Its orientation in the  $(k_x, k_y)$  plane can be tuned by simply rotating the sample. By investigating the properties of the collective excitations of a condensate polarized along the static field, we show that the gauge field makes the homogeneous superfluid flow unstable i) against transverse excitations in a limited region below  $k_*$  and ii) against both transverse and longitudinal excitations for wave vectors above  $k_*$ , depending on the condensate polarization. These two instability mechanisms trigger the formation of spin stripes and spin domain walls. A remarkable regime occurs when the polarization of the condensate is perpendicular to the static field. In such a case, a slowly propagating flow is unstable, whereas the superfluid motion is recovered above a critical velocity. This leads to an unexpected breakdown of superfluidity in the subsonic regime.

We consider the motion of a bosonic fluid governed by the spinor Gross-Pitaevskii equation

$$i\hbar \frac{\partial \Psi}{\partial t} = \hat{H}_0 + \alpha_1 \Psi^\dagger \Psi \Psi + \alpha_2 \Psi^\dagger \Psi \sigma_x \Psi, \quad (1)$$

where  $\Psi = (\psi_+, \psi_-)^T$ ,  $\alpha_1$  and  $\alpha_2$  are the intra- and inter-spin interactions, and  $\sigma_x$  is the anti-diagonal Pauli matrix. The single particle Hamiltonian, valid for both weakly coupled photons and polaritons in the parabolic approximation, is written as

$$\hat{H}_0 = \begin{bmatrix} -\frac{\hbar^2 \nabla^2}{2m} & -\frac{\Omega}{2} e^{-i\varphi} + \beta (\partial_y - i\partial_x)^2 \\ -\frac{\Omega}{2} e^{i\varphi} + \beta (\partial_y + i\partial_x)^2 & -\frac{\hbar^2 \nabla^2}{2m} \end{bmatrix}, \quad (2)$$

where  $\beta = \hbar^2/(4m_r)$  is the strength of the TE-TM field,  $m_\ell$  and  $m_t$  represent the longitudinal and transverse polariton masses,  $m_r = m_\ell m_t/(m_t - m_\ell)$  is the relative mass and  $m = (m_\ell + m_t)/2$  is the averaged polariton mass. The Hamiltonian (2) describes an ideal polariton BEC, in the limit of the very long life-time, decoupled from the thermal bath. Diagonalization leads to the following single-particle spectrum:

$$\epsilon_\pm = \frac{\hbar^2 k^2}{2m} \pm \sqrt{\beta^2 k^4 - \beta \Omega k^2 \cos(2\theta - \varphi) + \frac{\Omega^2}{4}}, \quad (3)$$

where  $k = \sqrt{k_x^2 + k_y^2}$  and  $\mathbf{k} = k(\cos \theta, \sin \theta)$ . Due to the anisotropy of the TE-TM field, the spectrum (3) encodes very interesting features, as summarized in Fig. 2. Let us take  $\varphi = 0$ , for a moment. For  $k_x < k_{c1}$ , with  $k_{c1} = \sqrt{2m_\ell \Omega/\hbar^2}$ , the energy is a monotonic function of  $k_y$  (Fig. 2b); on the other hand, for  $k_x > k_{c1}$  the lower branch  $\epsilon_-(k_y)$  bends and the parametric process  $k_y : 0 \rightarrow \pm \kappa_p \equiv [2mk_x^2/(2m_r - m) - 4\Omega m m_r/(\hbar^2(2m_r + m))]^{1/2}$  conserving both energy and momentum is possible (see Fig. 2c)). As a consequence, a transverse instability of the condensate becomes possible. More interestingly, the lower and upper branches cross each other at the wavevector  $k_* = \pm \sqrt{\Omega/2\beta}$  (see Fig. 2a)). At this specific point, the TE-TM and the applied fields compensate and the dispersion relation is locally isotropic and linear near  $q = 0$ ,  $\epsilon_\pm - \epsilon(k_*) \simeq \hbar^2 q^2/(2m) \pm \sqrt{\beta \Omega} q$ , with  $\mathbf{q} = \mathbf{k} - \mathbf{k}_*$ . This corresponds to dispersion of a system in the presence of spin-orbit coupling of the Rashba type. For arbitrary values of  $\varphi$ , such compensation takes place at the propagation wavevector  $\mathbf{k}_* = \pm \sqrt{\Omega/2\beta} (\cos \varphi/2, \sin \varphi/2)$ . Around this point ( $|q| \lesssim k_*$ ), the polariton Hamiltonian reads

$$\hat{H}_0 \simeq \frac{\hbar^2}{2m} (\mathbf{q}^2 + \kappa_x \boldsymbol{\sigma} \cdot \mathbf{q} + \kappa_y (\boldsymbol{\sigma} \times \mathbf{q}) \cdot \mathbf{e}_z), \quad (4)$$

where  $\kappa_x = 2m\sqrt{\beta \Omega}/\hbar^2 \cos \varphi/2$  and  $\kappa_y = 2m\sqrt{\beta \Omega}/\hbar^2 \sin \varphi/2$ . In opposition to TE-TM spin-orbit coupling in Eq. (2), the latter describes a true

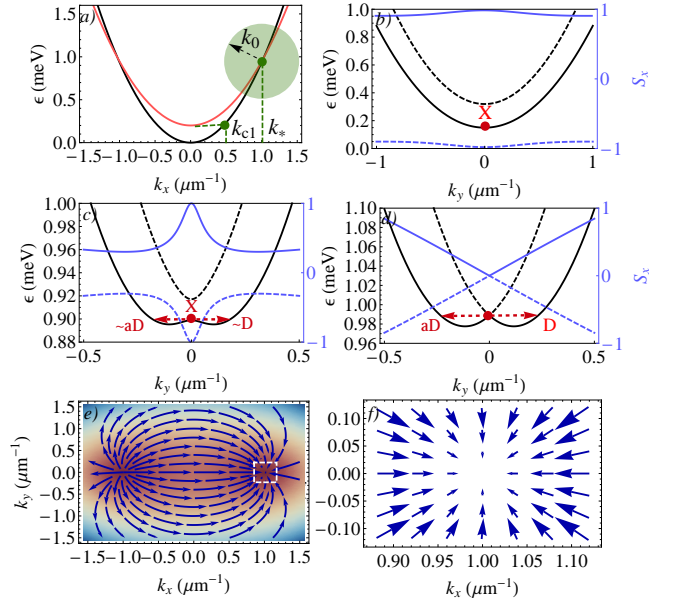


FIG. 2: (color online) Polariton dispersion relation for  $\varphi = 0$  (relative to  $\Omega/2$ ). a) Dispersion along the  $x$ -direction showing the two polariton branches  $\epsilon_\pm$  crossing at the magic point  $k_* = \sqrt{\Omega/2\beta}$ . The propagation wavenumber  $k_0$  defines a circle limiting the validity of the Hamiltonian (4). The critical point  $k_{c1}$  satisfies  $\epsilon_-(k_{c1}) = \epsilon_+(0) = \Omega$ . Panels b), c) and d) depict the dispersion along the  $y$ -direction, respectively for  $k_x = \{0.4, 0.97, 1.1\} \mu\text{m}^{-1}$ . In c), a parametric process  $k_y : 0 \rightarrow \pm \kappa_p$  occurs between a X-polarized mode and a diagonal (D) and an anti-diagonal (aD) modes. In d), we observe the signature of the gauge field, with the two branches touching each other at  $k_y = 0$ . Panel e) depicts the field texture of the off-diagonal terms in (2) in the reciprocal space and panel f) zooms around the compensation wavevector  $k_*$ . We have considered the following parameters:  $m = 4.5 \times 10^{-5} m_e$ ,  $\Omega = 0.2 \text{ meV}$  and  $\beta = 0.1 \text{ meV} \mu\text{m}^2$ .

gauge-field, minimally coupled Hamiltonian, where  $\kappa_x$  and  $\kappa_y$  represent the magnitude of the monopolar- and Rashba- field coupling constants. The gauge-field texture  $\mathbf{S}(\mathbf{k})$  for the particular case of propagation along a horizontal magnetic field ( $\theta = \varphi = 0$ ) is illustrated in panel e) and zoomed around  $\mathbf{k}_*$  in panel f) of Fig. 2. Because of the specific angular dependence of the TE-TM field, very different textures of the gauge field can be experimentally realized by simply rotating the sample. This results in more general field (or spin) textures, related by the transformation  $\mathbf{S}'(\mathbf{k}) = \mathcal{R}(\varphi) \mathbf{S}[\mathcal{R}(-\varphi/2) \mathbf{k}]$ , where  $\mathcal{R}(\varphi)$  is the  $2 \times 2$  rotation matrix (see the supplemental information in [23] for illustrative cases). Hereinafter, we consider the case  $\varphi = 0$  for definiteness. To illustrate the effect of gauge field (4) in real-life experiments, we consider photons (polaritons) propagating against a defect at the magic wave-number  $\mathbf{k}_0 = k_* \mathbf{e}_x$ . A cylindrical defect of size  $a$ , described by the potential  $U(r) = U_0 \exp(-r^2/a^2)$ , populates the states  $q_\pm = \pm 2\pi/a$ . The particles of the

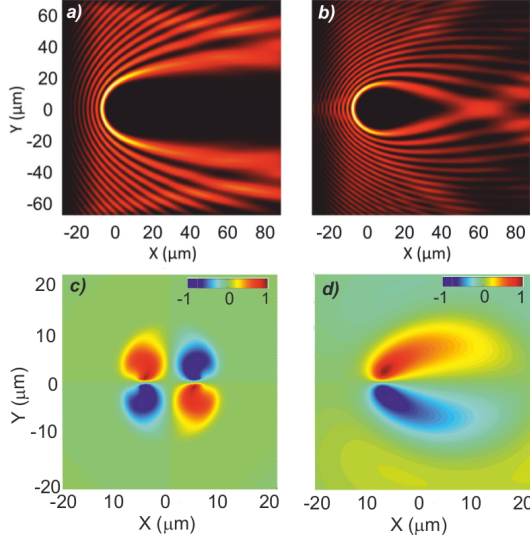


FIG. 3: (color online) Effects of gauge field for propagating polaritons. a) A flow passing an obstacle without fields ( $\beta = \Omega = 0$ ). b) Focusing effect in the presence of the monopolar gauge field of Fig. 2 f) at the magic point  $k_*$ . We have used the same field parameters of the Fig. 2 in both situations. Panels c) and d) depict the circular polarization degree after a laser pulse of duration 10 ps and spot  $5 \mu\text{m}$ , with a polariton life-time of 100 ps. c) Vertical incidence ( $\chi = 0$ ), showing the spin pattern related to the spin eigen-states of the TE-TM field [13]. Panel d), polaritons propagating at  $\mathbf{k}_0 = k_* \mathbf{e}_x$  ( $\chi \simeq 10^\circ$  for GaAs) exhibiting the two-fold spin pattern of in the presence of a gauge field.

mode  $q_y = q_+$  ( $q_y = q_-$ ) are pulled down (pushed up) (see [23] for details). In fact, the defect focuses the beam, as if light was “bent” by it (see Figs. 3a) and 3b)). This is quite remarkable, since focusing is obtained with an impenetrable defect. Another signature of a gauge-field, which can also be very easily observed in basic experimental setups, is the conversion of a four-fold spin pattern, associated with spin Hall effect due to the TE-TM field [13] into a two-fold spin pattern. In Figs. 3 c) and 3 d), we depict the circular polarization degree  $\rho_c = (n_+ - n_-)/(n_+ + n_-)$ , with  $n_\pm = |\psi_\pm|^2$ , for the case of a cw pulse of 10 ps pumping polaritons at  $\mathbf{k}_0 = 0$  and at the magic wave-vector  $\mathbf{k}_0 = k_* \mathbf{e}_x$ .

To include the interactions, we consider the dynamics of a polariton condensate propagating in the vicinity of the “magic” point  $k_*$ . The collective excitations of a polariton BEC propagating with velocity  $\mathbf{v}_0 = \hbar \mathbf{k}_0 / m$  can be investigated by linearizing (1) with the Bogoliubov prescription,  $\Psi = e^{i(\mathbf{k}_0 \cdot \mathbf{r} - \mu t / \hbar)} [\Psi_0 + \sum_{\mathbf{q}} (\mathbf{u}_{\mathbf{q}} e^{i(\mathbf{q} \cdot \mathbf{r} - \omega t)} + \mathbf{v}_{\mathbf{q}}^* e^{-i(\mathbf{q} \cdot \mathbf{r} - \omega t)})]$  [23], for a linearly polarized condensate,  $\Psi_0 = (n_+, n_-)^T = n_0 (e^{i\eta}, e^{-i\eta})^T$ , with  $\eta$  being the polarization angle, that corresponds to a state with magnetic energy  $E = -(1/2) \int d\mathbf{r} \Psi^\dagger \Omega \sigma_x \Psi$ . Therefore, a condensate is said to be X- (Y-) polarized for  $\eta = 0$

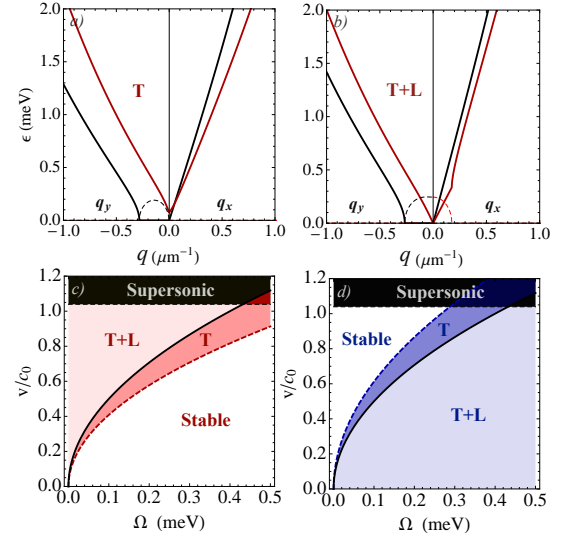


FIG. 4: (color online) Transverse (T) and longitudinal (L) instabilities for a X- polarized condensate with a blue-shift of  $\alpha_1 n = 1 \text{ meV}$  and  $\alpha_2 = -0.2\alpha_1$ . The solid and dashed lines respectively represent the real and imaginary parts of  $\epsilon_\pm$ . Panel a)  $k_{c1} < k_0 < k_*$ ; panel b)  $k_0 > k_*$ . Stability diagram for X- (panel c)) and Y-polarized (panel d)) condensates. The black solid line represents the velocity  $v_* = \hbar k_*/m$ , and the red/light grey (blue/light grey) dashed lines correspond to  $v_{c1} = \hbar k_{c1}/m$  ( $v_{c2} = \hbar k_{c2}/m$ ).

( $\eta = \pi/2$ ), and the associated pseudo-spin is  $\mathbf{S}_0 = n_0 \mathbf{e}_x$  ( $\mathbf{S}_0 = -n_0 \mathbf{e}_x$ ) [28]. The chemical potential contains the interaction and “magnetic” energy of the condensate

$$\mu = (\alpha_1 + \alpha_2) n_0 - \frac{1}{2} (\Omega - 2\beta k_0^2 \cos 2\theta) \cos 2\eta. \quad (5)$$

We consider a BEC propagating with wavevector  $\mathbf{k}_0 = k_0 \mathbf{e}_x$  and for which the non-linearity is large enough so the critical Landau velocity for the breakdown of superfluidity is larger than  $v_0 = \hbar k_0 / m$ . Let us discuss the case of a X-polarized BEC first (X is the ground state at  $q = 0$ ). For  $k_0 < k_{c1}$ , the dynamics of the condensate is stable, characterized by two modes  $\epsilon_\pm$ , which, in the long-wavelength limit  $q\xi \lesssim 1$  read

$$\begin{aligned} \epsilon_-(q_x) &\simeq c_-^x q_x, & \epsilon_+(q_x) &\simeq (\epsilon_0^2 + c_+^x{}^2 q_x^2)^{1/2} \\ \epsilon_-(q_y) &\simeq c_-^y q_y, & \epsilon_+(q_y) &\simeq (\epsilon_0^2 + c_+^y{}^2 q_y^2)^{1/2}, \end{aligned} \quad (6)$$

where  $\epsilon_0 = \epsilon_0(k_0, \Omega, \beta)$  is the gap energy at the origin and  $c_\pm^{x,y} = c_\pm^{x,y}(k_0, \Omega, \beta)$  represent speeds. For  $k_0 > k_{c1}$ , the two modes in the longitudinal direction become acoustic, i.e.  $\epsilon_\pm \simeq c_\pm^x q_x$ . Interestingly, along the transverse direction the lower mode becomes flat with a positive imaginary part (fig 4 a)), announcing the onset of an instability at  $q_y = 0$ , as a consequence of the parametric process of Fig. 1 c).

This purely transverse (T-) instability takes places in the interval  $0 < |q_y| < \kappa_p$ . The most unstable mode is

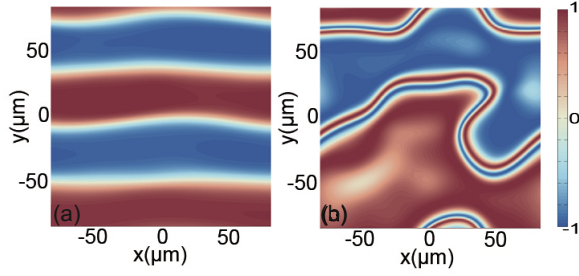


FIG. 5: (color online) Snapshots of the diagonal polarization degree  $\rho_D = (n_D - n_{aD})/(n_D + n_{aD})$  after the onset of instabilities in a X-polarized BEC.  $v/c_0 = 0.45$  (a) and  $v/c_0 = 0.6$  (b). We have considered the following parameters:  $m = 4.5 \times 10^{-5} m_e$ ,  $\Omega = 0.2$  meV and  $\beta = 0.1$  meV  $\mu\text{m}^2$ ,  $\alpha_1 n = 1$  meV and  $\alpha_2 = -0.2\alpha_1$ .

achieved for  $|q_y| = \kappa_p/2$ , at the point where the imaginary part of dispersion reaches its maximum (see Fig. 1 c)). Finally, for  $k_0 > k_*$ , the dynamics becomes unstable along the longitudinal direction as well (T+L-instability) as shown the 4 b). This is a consequence of the parametric process shown in Fig. 1 d). The most unstable mode, however, is now observed for  $(q_x, q_y) = (0, \kappa_p/2)$ , similar to the zero wave-vector instability discussed for atomic BECs (see e.g. Ref. [26]). The substantial difference is that here this instability is only achieved for a propagating (and not for a static) condensate. The phase diagram summarizing these results is depicted in Fig. 4 c). Increasing the velocity, the system evolves from superfluid to transversally, transversally and longitudinally unstable to finally reach the supersonic regime.

The case of a Y-polarized BEC is summarized in Fig. 4 d), and is even more intriguing. For very low wave-vectors, namely  $k_0 < k_{c1}$ , the spin is anti-aligned with the static field ( $\mathbf{S} = -n_0 \mathbf{e}_x$ ) and the system is T+L- unstable. Above the magic value  $k_*$ , the imaginary part of the energy vanishes in the  $x$  direction, and the system exhibits a purely transverse instability. At wave-vectors higher than the second critical wave-vector  $k_{2c} = \sqrt{2m_t\Omega/\hbar^2}$ , the system becomes stable. This counter-intuitive result simply states that superfluidity breaks down when the flow velocity is decreased or when particle density is increased.

To confirm the previous results, we performed numerical simulation using the spinor Gross-Pitaevskii Eq. (1). For a X-polarized condensate, we observe the formation of stripes along the transverse direction for  $k_0 > k_{c1}$ , illustrating the onset of a transverse instability (Fig 5 a)) and the formation of spin domain walls for  $k_0 > k_*$  by the T+L- instability mechanism (see Fig. 5 b)). Repeating the calculations for a Y-polarized BEC, the former is observed for  $k_* > k_0 > k_{c2}$  while the latter is obtained for  $k_0 < k_*$  (see the supplemental information [23]). At late stages, the instability saturates and the domain wall break into pair of half-vortices, the elementary topologi-

cal defects in spin-anisotropic BECs [16] (a movie is provided in [23]). For both polarizations, we observe that the formation of spin domain walls is much faster than the formation of stripes, which can be understood from the polarization of the excitations. The onset of transverse (longitudinal) instability is the consequence of a parametric process which populates the modes  $q_y = \pm\kappa_p$  ( $q_x = \pm\kappa_x$ ) from the initial state at  $(q_x, q_y) = (0, 0)$ . The efficiency of the process is proportional to  $\cos^2(2\Delta\eta)$ , where  $\Delta\eta$  is the relative polarization angle between the initial and final states [24, 25]. From Fig. 1, we observe that a process of the type  $q_y : 0 \rightarrow \pm\kappa_p$  occurs between an X- and two almost diagonal (D and aD) states, for which  $\Delta\eta \simeq \pi/4$  and  $\cos^2(2\Delta\eta) \ll 1$ . The longitudinal instability develops faster, since the process  $q_x : 0 \rightarrow \pm\kappa_x$  conserves polarization and, therefore,  $\cos^2(2\Delta\eta) = 1$ . Our results reveal a curious difference in respect with atomic BECs, where exotic phases are formed in static systems [22, 26, 27]. Here, instead, the gauge field is formed due to the balance between the TE-TM and the static fields, for which propagation is absolutely required. The configuration we propose is not only realistic, but is realized in any microcavity where both static and TE-TM induced fields are always present.

To conclude, we would like to discuss the possibility of engineering a quadratic spin-orbit term, similar to the TE-TM field, for the case of atomic BECs. The general scheme to synthesize a gauge field of the Rashba type is via Raman coupling between of the Zeeman splitted states  $m_F = -1$  and  $m_F = 0$ , belonging to a certain target state  $F = 1$ , in such a way that the state  $m_F = +1$  is far detuned. The effective gauge field, linear in  $k$ , results from a simple rotation of the Pauli matrices around to their axis (see Ref. [2] for details). If the Raman coupling targets the spin states  $m_F = \pm 1$ , with a far-detuned state  $m_F = 0$ , the rotating wave approximation and the reduction to a two-level problem would imply a double rotation of the Pauli matrices, and therefore a spin-orbit coupling quadratic in  $k$  and similar to our hamiltonian (2) would be possible for atoms. The achievement of a ‘TE-TM’ field for atomic condensates would be very interesting and would motivate the discussions between the two communities, leading to the observation of interesting topological effects like the nonlinear spin Hall effect [13].

We thank I. A. Shelykh for discussions. This work was supported by ‘‘ANR QUANDYDE’’, FP7 ITN ‘‘Spin-Optonics’’ (237252).

- 
- [1] Y.-J. Lin, R. L. Compton, K. Jiménez-García, J. V. Porto, and I. B. Spielman, *Nature* **462**, 628 (2009).
  - [2] Y.-J. Lin, K. Jiménez-García, and I. B. Spielman, *Nature* **471**, 83 (2011).
  - [3] M. Aidelsburger, M. Atala, S. Nascimbène, S. Trotzky,



- Y.-A. Chen, and I. Bloch, Phys. Rev. Lett. **107**, 255301 (2011).
- [4] S. Chen, J.-Y. Zhang, S.-C. Ji, Z. Chen, L. Zhang, Z.-D. Du, Y. Deng, H. Zhai, and J.-W. Pan, arXiv:1201.6018.
- [5] Y. K. Kato, R. C. Meyers, A. C. Gossard, and D. D. Awschalom, Science **306**, 1910 (2004).
- [6] M. König et al., Science **318**, 766 (2007).
- [7] C. L. Kane, and E. J. Mele, Phys. Rev. Lett. **95**, 146802 (2005).
- [8] B. A. Bernevig, T. L. Hughes, and S.-C. Zhang, Science **314**, 1757 (2006).
- [9] J. D. Koralek et al., Nature **458**, 610 (2009).
- [10] I.A. Shelykh, A.V. Kavokin, Y.G. Rubo, T.C.H. Liew, G. Malpuech, Semic. Sc.& Techn. **25**, 013001, (2010).
- [11] A. Kuther, M. Bayer, T. Gutbrod, A. Forchel, P. A. Knipp, T. L. Reinecke, and R. Werner, Phys. Rev. B **58**, 15744 (1998).
- [12] L. Klopotoski, M. D. Martin, A. Amo, L. Vina, I. A. Shelykh, M. M. Glazov, G. Malpuech, A. V. Kavokin, and R. Andre, Solid State Com., **139**, 511 (2006).
- [13] H. Flayac, D. D. Solnyshkov, I. A. Shelykh, and G. Malpuech, Phys. Rev. Lett. **110**, 016404 (2013).
- [14] A. Kavokin, G. Malpuech, and M. Glazov, Phys. Rev. Lett. **95**, 136601 (2005).
- [15] C. Leyder, M. Romanelli, J. Ph. Karr, E. Giacobino, T. C. H. Liew, M. M. Glazov, A. V. Kavokin, G. Malpuech, A. Bramati, Nature Physics **3**, 628 (2007).
- [16] D. D. Solnyshkov, H. Flayac, and G. Malpuech, Phys. Rev. B **85**, 073105 (2012).
- [17] R. Hivet, H. Flayac, D.D. Solnyshkov, D. Tanese, T. Boulier, D. Andreoli, E. Giacobino, J. Bloch, A. Bramati, G. Malpuech, A. Amo, Nature Physics **8**, 724 (2012).
- [18] I. A. Shelykh, Y. G. Rubo, G. Malpuech, D. D. Solnyshkov, and A. Kavokin, Phys. Rev. Lett. **97**, 066402 (2006).
- [19] J. Dalibard, F. Gerbier, G. Juzeliūnas, P. Öhberg, Rev. Mod. Phys. **83**, 1523 (2011).
- [20] Y. A. Bychkov and E. I. Rashba, J. Phys. C **17**, 6039 (1984).
- [21] G. Dresselhaus, Phys. Rev. **100**, 580 (1955).
- [22] S. Sinha, R. Nath, and L. Santos, Phys. Rev. Lett. **107**, 270401 (2011).
- [23] See Supplemental Material for a schematic explanation of the lensing effect and further details on the linearization of Eq. (1).
- [24] A. Kavokin and G. Malpuech, 5th chapter of Cavity Polaritons, Edited by V.M. Agranovich, Elsevier (2003).
- [25] I. Carusotto, and C. Ciuti, Rev. Mod. Phys. **85**, 299 (2013).
- [26] C. Wang, C. Gao, C-M. Jian, and H. Zhai, Phys. Rev. Lett. **105**, 160403 (2010).
- [27] H. Hu, B. Ramachandhran, H. Pu, and X-Ji Liu, Phys. Rev. Lett. **108**, 010402 (2012).
- [28] H. Flayac, D. D. Solnyshkov and G. Malpuech, Phys. Rev. B **83**, 193305 (2011).